Journal of Applied Physics ARTICLE pubs.aip.org/aip/jap

Formation and stability of point defect color centers in 6H silicon carbide

Cite as: J. Appl. Phys. **135**, 225701 (2024); doi: 10.1063/5.0205832
Submitted: 28 February 2024 · Accepted: 25 May 2024 ·
Published Online: 10 June 2024

Erlend Lemva Ousdal,[a] Marianne Etzelmüller Bathen, Augustinas Galeckas, Andrej Kuznetsov, and Lasse Vines

AFFILIATIONS

Department of Physics/Centre for Materials Science and Nanotechnology, University of Oslo, 0316 Oslo, Norway

Note: This paper is part of the special topic, Defects in Semiconductors 2024.
[a]**Author to whom correspondence should be addressed:** erlendou@uio.no

ABSTRACT

Point defect color centers acting as single-photon emitters are promising for quantum technology applications and have been extensively studied, e.g., in the 4H polytype of silicon carbide (SiC). However, the physics of such color centers in other SiC polytypes is much less explored. Herein, we study the formation and thermal stability of such color centers in 6H-SiC using photoluminescence spectroscopy. The emissions from typical single-photon emitters, such as silicon vacancies, divacancies, and carbon antisite-vacancy pairs in 6H-SiC, were monitored as a function of the proton irradiation fluence and post-irradiation annealing, and compared to that in 4H-SiC. Overall, at the background of similarities between the emission behavior in 4H- and 6H-SiC polytypes, we observed prominent differences; e.g., for the thermal stability of the carbon antisite-vacancy pair, which exhibited maximized emissions upon 300 and 900 °C anneals in 4H- and 6H-SiC, respectively. Moreover, we observed a range of defect emission signatures not previously reported for 6H-SiC in the literature and discussed their potential origin in the context of the thermal stability. For example, among the PL-lines in 6H-SiC, we detected periodically repeatable emission signatures, resembling the so-called L-lines recently reported in 4H-SiC, even though their exact origin has not yet been settled in the literature. Thus, we use color centers comparison in different polytypes to better understand the nature of the single-photon emitters in SiC.

I. INTRODUCTION

Silicon carbide (SiC) is a wide-bandgap semiconductor that is used in various technological areas for its functional and structural properties, such as the wide band gap, high hardness, and large critical breakdown field. Perhaps, the most important application of SiC at the moment is its use in power electronics, as SiC offers a promising platform to produce devices which are suitable for high temperature, high frequency, and high voltage applications.[1] However, deep-level defects in SiC material still hinder the performance of power devices, including the carrier lifetime limiting effect of point defects such as the carbon vacancy[2,3] and boron impurities,[4] extended defects that contribute to limited radiation hardness of SiC power devices,[5] and defects at the SiO_2-SiC interface that enhance channel resistance and contribute to losses in the SiC MOSFETs.[6] Therefore, detailed defect studies are of paramount importance to SiC technology.

In quantum technology (QT), on the other hand, point defects can be utilized beneficially, as they can act as sources of single photons or spin qubits embedded in a solid state matrix. Over recent years, SiC has begun receiving widespread attention for its possible use as a platform for QT.[7] Thus, being able to reproducibly generate, control, and tune defect species is of great importance. Defects such as the Si vacancy (V_{Si}), carbon antisite-vacancy pair ($C_{Si}V_C$ or CAV), divacancy ($V_{Si}V_C$ or VV), and nitrogen-vacancy (N_CV_{Si} or NV) center in 4H-SiC have been demonstrated as room temperature single-photon emitters (SPEs)[8–11] with coherent single spin control demonstrated for all except for the CAV complex. By controlling emission from quantum compatible point defects, it is possible to use the emitted photons as quantum information for many purposes, such as quantum communication, sensing, and as qubits for quantum computing. Additionally, the long lived spin state of a charge carrier localized at such a deep-level defect is of

interest as spin qubits for quantum computing, quantum sensor objects, and quantum memories. The semiconductor platform for QT offers many benefits over potentially competing technologies, such as possibility of room temperature operation and the benefit of having an already existing and mature infrastructure because of, e.g., silicon technology and SiC based power electronics.

SiC can exist in over 200 different polytypes.[12] Among these, the 4H configuration with 50% hexagonality is the most widely used for both QT and power electronics applications, because of its favorable properties and high quality material fabrication. However, this does not mean that the point defects in 4H-SiC are necessarily the most suitable when considering quantum applications. Another polytype with similar defects to 4H is 6H-SiC. In addition to having similar defects to the ones observed in 4H, 6H-SiC has two more layers per stacking sequence, resulting in additional possible configurations for each defect. The defects that have been studied for the purpose of QT in SiC, such as the V_{Si}, $C_{Si}V_C$, and $V_{Si}V_C$, are located at different energies in the bandgap in different polytypes of SiC, which again depends on the different atomic configurations due do different stacking sequences of the material. The polytype variation in SiC thus enables emission from a wide range of wavelengths from different defect complexes and stacking combinations.

In this work, we study the formation and evolution of the three defect types V_{Si}, $C_{Si}V_C$, and $V_{Si}V_C$ in the 6H polytype of SiC. Their behavior as a function of proton irradiation fluence and post irradiation annealing temperature is compared to the behavior of the equivalent defects in 4H-SiC. The samples are studied using photoluminescence (PL) spectroscopy and capacitance–voltage (C–V) measurements. We identify optimal formation conditions for the defect complexes and find notable differences between the defects embedded in the two SiC polytypes. Additionally, we report new signatures of unknown origin that to our knowledge have not previously been reported in the PL-spectrum of 6H-SiC.

II. METHODOLOGY

We employ n-type nitrogen doped epitaxial (epi-layer) samples of both 6H- and 4H-SiC. The 6H-SiC wafer was produced by SiCrystal AG with a carrier concentration that varied in the range of 1×10^{17}–1×10^{20} cm^{-3}, as determined using C–V measurements. The thickness of the 6H epi-layer was 5–6 μm as determined by cross-sectional scanning electron microscopy (SEM) imaging. The 4H-SiC wafers are purchased from CREE/Wolfspeed and had a lower net carrier concentration of $\sim 1 \times 10^{15}$ cm^{-3} in the 10 μm thick epi-layer as measured by C-V. For the 4H wafer, the epi-layer was grown on top of a highly doped ($\sim 8 \times 10^{18}$ cm^{-3}) n-type 4H-SiC substrate. This means that the carrier concentration in the 6H sample is less uniform than in the 4H sample, but we do not expect this to affect the validity or uncertainty of the measurements.

The different doping densities give rise to small differences in Fermi level (E_F) with E_F being 0.13 and 0.09 eV below the conduction band edge in the 4H- and 6H-SiC samples, respectively, at room temperature. Although the Fermi level is expected to contribute to both variations in formation probability[13] and emission intensity[14] for defects like, e.g., the V_{Si}, such small differences in Fermi level are not expected to have pronounced impact for the PL measurements performed herein.

To form defect complexes, the samples were irradiated with 1.8 MeV protons at room temperature with fluences in the range of 5×10^{13}–1×10^{15} cm^{-2}, using a titanium hydride source for the protons. After irradiation, the samples were annealed in a tube furnace using a SiC tube under Ar-flow at temperatures in the range of 300–1500 °C for a duration of 30 min. The high-temperature anneals were performed in the absence of the graphitized photoresist known as a carbon cap (C-cap) that is typically employed to protect the SiC surface during high-temperature annealing.[15,16] This was to avoid injection of C interstitials (C_i) that may form electrically active defects and complex with or annihilate the vacancy-related defects that are the subject of this study.[17,18] The absence of a C-cap during annealing $\geq$1000 °C may contribute to changes in surface stoichiometry after high-temperature annealing, but that is not expected to influence the photoluminescence measurements performed herein as the entire epitaxial layer (10 and 5–6 μm for the 4H- and 6H-SiC, respectively) is probed. The 300 °C anneal is expected to contribute to clearing out of interstitial defects induced by irradiation while higher temperature heat treatments can promote complex formation driven by atomic hops and defect migration.

The defect emission was monitored using PL spectroscopy at cryogenic temperatures and in spectral windows where emissions from the V_{Si}, $C_{Si}V_C$, and $V_{Si}V_C$ in 4H- and 6H-SiC are expected, based on the literature. We additionally investigate the full spectrum in the range 550–1200 nm to monitor the appearance of new defect signatures upon proton irradiation and/or the disappearance of those related to the V_{Si}, $C_{Si}V_C$, and $V_{Si}V_C$. Note that the probing depth of the excitation beam exceeds the thickness of the epi-layers in both 4H- and 6H-SiC; however, we assume the measured emission to originate from defects in the epi-layer and not the substrate. This is because the excitation beam is focused on the surface of the sample with an incident angle which means that most of the laser intensity is directed to the epi-layer. In addition, the high carrier concentration in the substrate leads to a higher probability of non-radiative recombination which leads to less luminescence from the substrate as compared to the epi-layer. Although some contribution to the measured PL signal from the substrate cannot be excluded, this will be the same for 4H samples (grown on 4H substrate) and 6H samples (grown on 6H substrate) and is not expected to influence our conclusions.

The samples were placed inside a closed-cycle He refrigerator system (CCS-450 Janis Research, Inc.) and all PL measurements were performed at 10 K. The PL measurements were performed using an iHR320 imaging spectrometer with a H10330C-75 photomultiplier tube. Excitation was achieved using a 405 nm solid state laser and using a 550 nm longpass filter. The laser power density is approximately 1 kW/cm^2 to be able to produce a sufficient signal without saturating the detector. All data shown in the paper are processed as to remove artifacts and baseline from the measurement setup.

For electrical measurements to determine the net carrier concentration in the samples, Schottky barrier diodes (SBDs) were fabricated by depositing 100 nm thick Ni contacts using electron beam evaporation following a HF dip (1 min) to remove the native oxide. The SBD contacts are circular with 100 μm diameter. The electrical characterization by C-V measurements was carried out using a

Boonton-7200 high-precision capacitance meter, operating at a test frequency of 1 MHz.

III. RESULTS AND DISCUSSION

Table I summarizes three main defects studied herein ($C_{Si}V_C$, V_{Si}, and $V_{Si}V_C$) and their expected zero phonon line (ZPL) energies in 4H- and 6H-SiC. For the V_{Si}, we expect ZPLs of emission in the 858–920 nm range for both the 4H and 6H polytype cases. The $C_{Si}V_C$, on the other hand, exhibits ZPLs around 648–680 nm in 4H-SiC, with the corresponding emission lines in 6H-SiC landing around 740–770 nm. In both 4H- and 6H-SiC, the $V_{Si}V_C$ related ZPLs are situated in the spectrum around 1078–1140 nm. As demonstrated in Table I, there are more possible configurations in 6H than in 4H-SiC. This is because of the different crystal structures in the two polytypes. 4H-SiC has two unequal lattice configurations, the hexagonal (h) and the pseudo-cubic (k). This means that there are two possibilities for defects like the V_{Si} (h corresponding to the V1 and V1', and k corresponding to the V2 configuration[27]), and four possible configurations for defects like the $V_{Si}V_C$ (hh, kk, hk, and kh, corresponding to PL1-PL4, respectively[28]) and $C_{Si}V_C$ (assigned to the AB-lines[8,29]). 6H-SiC, with 33% hexagonality, has three distinct lattice sites and thus three configurations of mono-site defects like the V_{Si}: one hexagonal (h, corresponding to V1) and two cubic ones (k_1 and k_2, corresponding to V3 and V2, respectively).[26] This results in as much as six different configurations for double-site defects like the divacancy (k_2k_2, hk_2, k_2k_1, k_1h, hh, and k_1k_1, which correspond to QL6-QL1, respectively[26]).

ZPLs from defect SPEs embedded in 6H-SiC are mostly red-shifted compared to the corresponding ZPLs in 4H-SiC (see Table I). This could possibly be explained by the bandgap energy, which is 3.26 and 3.0 eV for 4H and 6H SiC, respectively.[30] Evidently, there are differences between the same defect types embedded in 6H- and 4H-SiC when considering their emission energies. Other defect properties, such as formation, annealing behavior, photon statistics, and spin dynamics, could be similarly varying for different SiC polytypes. Strictly quantum-related properties, such as spin control and single-photon characteristics, are outside the scope of this study, but worth keeping in mind as a motivational factor for further studies on color centers in 6H-SiC. Herein, we focus on comparing the dependence of defect-related emission as a function of the formation conditions (proton irradiation fluence), and their behavior upon post-irradiation heat treatments. It is important to note that in what follows, the emission intensities of all defects have been normalized to the maximum intensity for the given defect. This means that results are presented as relative values, and comparing absolute brightness of the defects is not possible from the results as they are presented here.

Figure 1 plots ZPL emission magnitudes for $V_{Si}V_C$ (top panels), V_{Si} (middle panels) and $C_{Si}V_C$ (bottom panels) as a function of the proton irradiation fluence for different anneals (left column), and on the annealing temperature for the 1×10^{15} cm^{-2} proton fluence (right column) in 6H- and 4H-SiC. As stated in Sec. II, the samples were proton irradiated with 1.8 MeV at either 5×10^{13} cm^{-2}, 1×10^{14} cm^{-2}, 5×10^{15} cm^{-2} or 1×10^{15} cm^{-2} fluence, and annealed after irradiation at 300–1500 °C for 30 min to enable defect migration and ensure complex-formation. We immediately observe that the evolution with annealing temperature differs widely between different defect types, and configurations within each defect type, while the proton fluence dependencies are more cohesive. In the following, we discuss the formation and stability of $V_{Si}V_C$, V_{Si}, and $C_{Si}V_C$.

TABLE I. Overview of emission wavelength (ZPL) for the main defect signatures studied in this work, in both 4H- and 6H-SiC, including commonly used labeling in the literature. The notation "x" means that the specific defect configuration has not been reported in that material. The column to the right specifies what figures in the text show the PL-signal of that defect.

Defect (Name)	6H (nm)[a]	4H (nm)[a]	6H in Fig.
CAV (A1)[19]	741.1[19]	648.1[19,20]	x
CAV (A2)[19]	747.6[19]	651.7[19,20]	x
CAV (A3)[19]	751.5[19]	x	x
CAV (B1)[19]	757.9[19]	671.6[19,20]	x
CAV (B2)[19]	760.1[19]	672.85[19,20]	4
CAV (B3)[19]	764.4[19]	675.1[19,20]	4
CAV (B4)[19]	768.9[19]	676.4[19,20]	4
V_{Si} (V1/V1')[21,22]	865/864.5[21,22]	861/858[21–23]	3
V_{Si} (V2)[21,22]	887[21,22]	917[20,22,24]	3
V_{Si} (V3)[21,22]	906.5[21,22]	x	3
V_CV_{Si} (QL6/PL4)[25]	1093[26]	1078[25]	2
V_CV_{Si} (QL5/PL3)[25]	1093.5[26]	1108[25]	2
V_CV_{Si} (QL4/PL2)[25]	1108[26]	1131[25]	2
V_CV_{Si} (QL3/PL1)[25]	1124[26]	1132[25]	2
V_CV_{Si} (QL2)[25]	1135[26]	x	2
V_CV_{Si} (QL1)[25]	1140[26]	x	2

[a]As found by photoluminescence measurements in the literature.

A. Evolution of the divacancy complex

The evolution of VV-related emission in 4H- and 6H-SiC is illustrated in the top panels of Fig. 1. It is observed (right topmost panel of Fig. 1) that emission from divacancy defects is by far at its brightest after annealing at 900 °C in both the 4H and 6H polytypes. Interestingly, the PL intensity is only a few percentages before and after annealing at this bright state. In 4H-SiC, the formation of VV has typically been related to the stability of $V_{Si}^-(k)$,[31] and we note that 6H-SiC behaves similarly.

Figure 2 shows the PL emission from V_CV_{Si}-related ZPLs in 6H-SiC for varying proton irradiation fluences in the range 5×10^{13}–1×10^{15} cm^{-3} and after the 900 °C anneal (with the highest emission intensity). As shown in Fig. 2, there are six ZPLs (QL1-QL6) assigned to different configurations of the divacancy in 6H-SiC. As mentioned above, the k_2k_2, hk_2, k_2k_1, k_1h, hh, and k_1k_1 configurations of the divacancy have been assigned to the QL6-QL1 ZPLs, respectively.[26] Note that the QL5 and QL6 are closely spaced (see the inset of Fig. 2). We are able to decouple the two in some measurements, but not all. Thus, they are treated as one peak when we consider their behavior in Fig. 1. It should still be noted that QL5 and QL6 respond differently to the temperature and fluence and that QL6 is the strongest contributor to the QL5/QL6 peak.

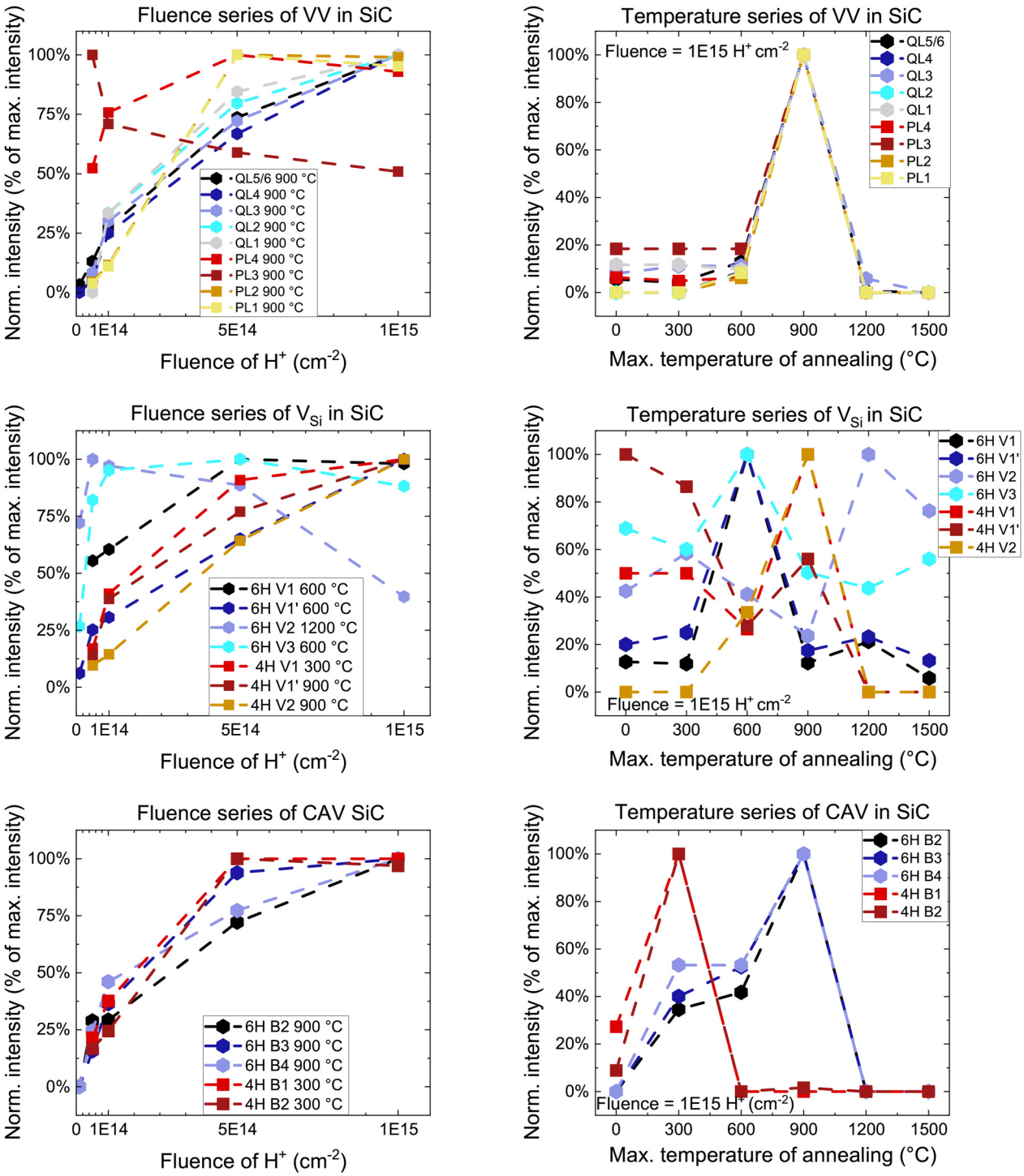

FIG. 1. ZPL emission magnitudes for $V_{Si}V_C$ (top), V_{Si} (middle), and $C_{Si}V_C$ (bottom) as a function of the proton irradiation fluence (left) and annealing temperature (right) in 6H- and 4H-SiC. Each data point is normalized with respect to the maximum intensity for that sample, meaning that 100% is the strongest signal from that sample, and other measurement intensities are given as a percentage of this intensity. This means that it is not possible to compare the relative intensity of different defects or the same defect within different samples.

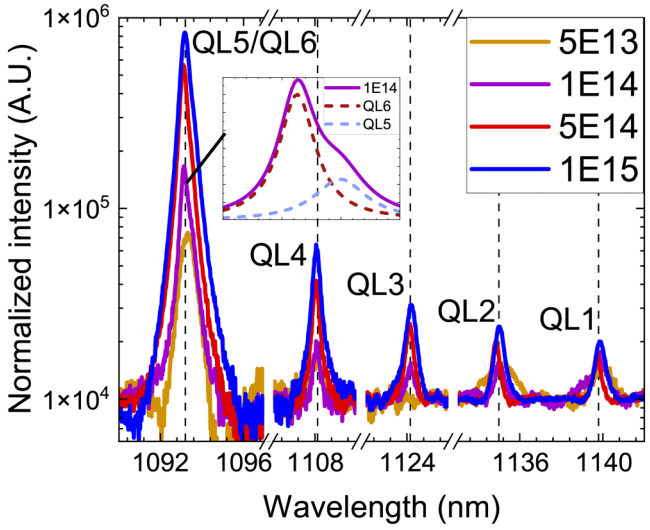

FIG. 2. PL emission at 10 K focusing on the QL1-QL6 ZPLs assigned to the divacancy in 6H-SiC for different proton irradiation fluences in the 5×10^{13}–1×10^{15} cm^{-2} range. The samples were annealed at 900 °C for 30 min in Ar-flow. The inset shows the close overlap of QL5 and QL6 for the 1×10^{14} cm^{-2} sample.

Figure 2 (and the top left panel of Fig. 1) demonstrates that the emission intensities from the divacancy configurations increase as a function of proton fluence for all 6H-divacancies (QL1–QL6). This is to be expected as higher-fluence irradiation creates more monovacancies of both the silicon and carbon types, which are the constituents of the VV complexes. Note that the samples in Fig. 2 were all annealed at 900 °C for 30 min as to allow for migration of the V_{Si}, leading to encounters with stationary V_C (below ~1200–1500 °C[32]) and causing formation of the $V_{Si}V_C$. For two of the divacancies in the 4H SiC polytype, however, the behavior is rather different (see the top left panel of Fig. 1). PL4 does not change as strongly as the others from the lowest to the highest fluence, and PL3 actually decreases in intensity as a function of proton fluence. This is particularly interesting as it shows differences in formation mechanisms between 4H- and 6H-SiC.

In summary, it seems that an annealing at around 900 °C is absolutely essential for creating a high density of divacancies in both 6H- and 4H-SiC. Previous results have shown this temperature to be closer to 800 °C;[33] however, as we measure at equidistant temperatures, the closest temperature we measure at is 900 °C. Variations due to different local sample processing conditions should also be taken into account.

B. Evolution of silicon monovacancies

The silicon vacancy has been studied extensively in 4H-SiC, where it exhibits two configurations with three ZPLs: V1 and V1' assigned to different excited states of the negatively charged V_{Si} on a hexagonal lattice site, $V_{Si}^{-}(h)$, and V2 assigned to the cubic $V_{Si}^{-}(k)$.[23,27] In 6H-SiC, there is one more V_{Si} configuration as compared to that of 4H-SiC. In 6H-SiC, V1 and V1' are assigned to the $V_{Si}^{-}(h)$, while V2 and V3 are assigned to the pseudo-cubic configurations, k_2 and k_1, respectively.[26] PL measurements revealing the dependence of these defect configurations in 6H-SiC (V1, V2, and V3) on proton irradiation fluence for the 600 °C heat treatment case are shown in Fig. 3. Figure 3 also demonstrates the presence of V1', which is by far the strongest signal in all measurements. As the emission lines from V1 and V1' are so spectrally close, and much closer than that in 4H, it is difficult to decouple their intensities; thus, the intensity from V1 is associated with a sizeable uncertainty.

It has been demonstrated that the optical signals from the silicon vacancies are strongly polarized, as V1' and V3 emit strongly along the *c*-axis (001), and V1 and V2 emit strongly perpendicularly to the c-axis.[34] The difference in polarization must be taken into account when considering the differences in intensity of the silicon vacancies in Fig. 3, as it can explain why V1' and V3 appear brighter than V1 and V2.

Figures 1 and 3 show that the configuration of the silicon vacancy determines its temperature and fluence dependencies. V1, V1', and V3 in 6H-SiC are brightest after heat treatment at 600 °C and exhibit relatively low intensities for all other temperatures (see the middle right panel of Fig. 1). This is different to the behavior of equivalent defects in 4H-SiC, as the V1' ZPL in the 4H polytype is most intense in the as-irradiated sample before any annealing, while V1 and V2 exhibit the strongest signals after an annealing at 900 °C.

The brightness of V2 in 6H-SiC is fairly stable for all annealing temperatures, but V2 is the only defect in this study that is the brightest after annealing above 900 °C (see Fig. 1). This suggests that complexes that form in 6H-SiC above 900 °C and have silicon

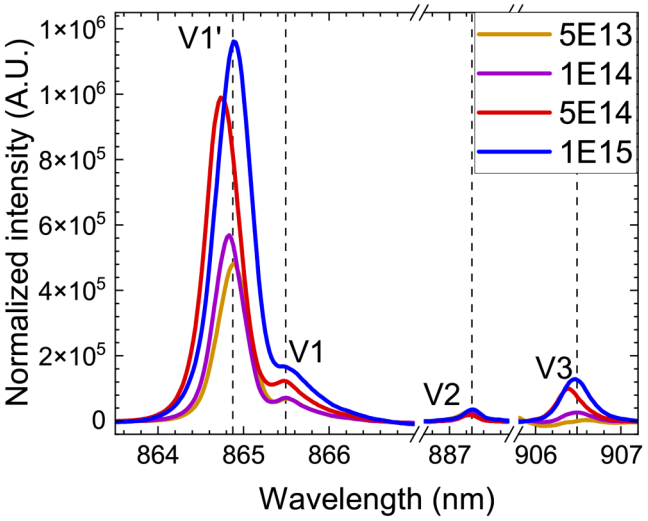

FIG. 3. PL emission at 10 K focusing on the V1–V3 ZPLs assigned to the V_{Si} in 6H-SiC for different proton irradiation fluences in the range of 5×10^{13}–1×10^{15} cm^{-2}. The samples were annealed at 600 °C for 30 min in Ar-flow.

vacancies as one of the constituents primarily include V1 and V3. The observation is supported by the fact that the only divacancy that is observable in 6H-SiC after annealing at temperatures above 900 °C is the QL3, which consists of the lattice site h and k_1, thus not involving V2 which is assigned the k_2 lattice site.

As for the fluence dependency of the silicon vacancies (the left middle panel of Fig. 1), we also observe a clear difference between the two polytypes. In 6H-SiC, for V2 and V3 with pseudo-cubic configurations,[26] the intensity increase saturates at a proton fluence of 5×10^{13} cm^{-2}. For the other silicon monovacancies in both 4H and 6H SiC, their intensities increase linearly to the logarithm of the fluence, reaching their highest intensity values at 1×10^{15} cm^{-2} protons. The reason for the early saturation of the intensity of the silicon vacancies at pseudo-cubic lattice sites may be because of non-radiative recombination sites that affect the emission from these defects more than they do the other silicon vacancies.

V2 in 6H-SiC is also the only of the V_{Si} configurations that exhibits a substantial decrease in brightness as fluence increases, as can be seen in Fig. 1 (middle left panel). This suggests that either the formation or the emission mechanism for the V2 in 6H-SiC is different than for the other silicon vacancies (V1 and V3). Note that this is only true for the sample annealed at 1200 °C, while for other temperatures, such as the one shown in Fig. 3 (annealed at 600 °C), the temperature dependency of V2 is more similar to that of V1 and V3. Note also that the V2 defect in 6H-SiC does not correspond to the V2 configuration in 4H. In fact, it is expected that the V2 emission in 6H arises from the k_2 lattice site,[26] which is not present in 4H-SiC. This may be a contributing factor in why the V2 center in 6H-SiC behaves differently than all the other silicon vacancies in both the 4H and 6H polytypes of SiC.

C. Evolution of the carbon antisite-vacancy pair

The carbon antisite-vacancy pair, or $C_{Si}V_C$, has four configurations, and six potential luminescence lines, in 4H-SiC (hh, kk, hk, and kh). Similarly, in 6H-SiC, there are six distinct CAV complexes (k_2k_2, hk_2, k_2k_1, k_1h, hh, and k_1k_1), with multiple sharp luminescence lines being observed. The CAV complexes in both 4H- and 6H-SiC result in what has previously been named the AB-lines (see Table I for wavelength values).[29] As there are more ZPLs than configurations in both 4H- and 6H-SiC, it is speculated that some of these arise from higher-lying excited states of the different CAV configurations. However, the identities of the individual lines are, to the best of our knowledge, not unambiguously determined.

The observed emission intensities related to the CAV complex have been low in both the 4H- and 6H-SiC samples studied in this work. As the CAV pair is known as a bright quantum emitter, as compared to, e.g., V_{Si} and divacancy defects,[8–10] this indicates lower probabilities of CAV formation in the present samples. A possible explanation is that we are using strongly n-type doped samples, where the CAV pair is known to be unstable with respect to the transformation into the V_{Si}, being preferred in n-type SiC material.[13] In 6H-SiC, only the B2, B3, and B4 ZPLs were observed with a sufficient intensity above the noise level herein (see Fig. 4), while the B1 and B2 emission lines were the most prominent in 4H-SiC.

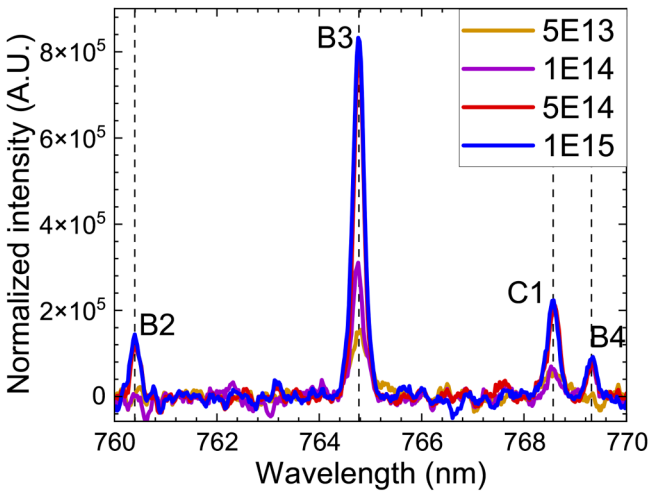

FIG. 4. PL emission at 10 K for the B2, B3, and B4 ZPLs related to the $C_{Si}V_C$ in 6H-SiC for different proton irradiation fluences in the 5×10^{13}–1×10^{15} cm^{-2} range. The samples were annealed at 900 °C in Ar-flow for 30 min.

Figures 4 and 1 (the lower left panel) demonstrate that the CAV pair increases in emission intensity as a function of proton fluence in both 4H and 6H-SiC, with a saturation effect being visible for higher fluences for some configurations. In addition to three CAV-peaks, the PL spectrum in Fig. 4 (for 6H-SiC) shows a fourth peak that has been labeled C1. This peak has currently no known origin assignment and behaves differently from the CAV-defects and is, therefore, expected to arise from a defect of different origin.

The results shown in the lower right panel of Fig. 1 demonstrate that the polytype has a strong impact on determining the temperature evolution of CAV-related defects. The behavior of CAV pairs within a polytype is almost identical. In 4H-SiC, the emission intensity from the CAV complex increases from as-implanted and reaches its brightest after a 300 °C anneal, after which it disappears below the detection limit of the PL setup. In 6H-SiC, on the other hand, a gradual increase in brightness is observed for each annealing step leading up to 900 °C, after which the CAV defects can no longer be observed in 6H-SiC either.

It is also interesting to see that the brightest emission from the CAV complexes in 4H-SiC appears at lower temperatures than the temperature at which the strongest signal from V1 and V2 is observed. In 6H-SiC, the highest concentration of CAV defects is observed at higher temperatures than the temperature at which the strongest signal from V1, V1', and V3 (being the equivalent silicon vacancies to V1 and V2 in 4H-SiC) is observed.

All CAV-defects in 6H-SiC become brighter with a higher fluence of protons, as expected for higher defect concentrations. In 4H-SiC, the brightness saturates at a proton fluence of 5×10^{14} cm^{-2} and does not increase further after this. This indicates a fluence-dependent interplay between radiative and non-radiative recombination channels.

D. Unidentified defect signatures in 6H-SiC

In addition to the VV, V_{Si}, and CAV defects that have been discussed so far, a considerable amount of sharp luminescence lines were discovered in a wide range of wavelengths in the 6H-SiC samples, as listed in Table II. For several of these lines, clear identification is missing in the literature. Interestingly, all the sharp PL lines observed herein are affected by the proton irradiation, indicating that they are somehow related to intrinsic defects and not impurities alone. A full characterization of these emission lines is beyond the scope of this paper; however, some analysis of possible origins interconnected to the defect stability is outlined below.

TABLE II. Summary of emission wavelengths and sample preparation parameters for unknown defects observed after 1.8 MeV proton irradiation and annealing of 6H-SiC.

Emission wavelength (nm)	Proton fluence (cm^{-2})	Annealing temperature (°C), 30 min
571.2	5×10^{14}[a]	1200
586.5	5×10^{14}[a]	900–1200
591.4	5×10^{14}[a]	1200
606.8	5×10^{14}[a]	1200
614.7	5×10^{14}[a]	1200
615.4	5×10^{14}[a]	1200
617.8	5×10^{14}[a]	1200
621.7	5×10^{14}[a]	1200
623.6	5×10^{14}[a]	1200
631.8	5×10^{14}[a]	1200
663.5	5×10^{14}[a]	900 & 1200
671.6	5×10^{14}[a]	0
746.7	$5 \times 10^{14} - 1 \times 10^{15}$	900
762.9	$5 \times 10^{14} - 1 \times 10^{15}$	1200
768.6	$1 \times 10^{14} - 1 \times 10^{15}$	900
822.2	5×10^{14}[a]	0
855.0	$5 \times 10^{13} - 1 \times 10^{15}$	0
873.8	$5 \times 10^{13} - 1 \times 10^{15}$	0–300
875.7	$5 \times 10^{13} - 1 \times 10^{15}$	0–300
876.8	$5 \times 10^{13} - 1 \times 10^{15}$	0–300
877.6	$5 \times 10^{13} - 1 \times 10^{15}$	0–300
885.2	5×10^{14}[a]	0
1095.7	$5 \times 10^{13} - 5 \times 10^{14}$	1500
1100.6	5×10^{14}[a]	1200
1105.1	5×10^{14}[a]	1200
1108.0	5×10^{14}[a]	900
1119.9	5×10^{14}[a]	1200
1123.0	5×10^{14}[a]	1200
1129.1	$5 \times 10^{14} - 1 \times 10^{15}$	1200
1134.0	5×10^{14}[a]	900
1144.3	$5 \times 10^{14} - 1 \times 10^{15}$	1200
1146.8	$5 \times 10^{14} - 1 \times 10^{15}$	1200
1162.7	5×10^{14}[a]	1200
1173.1	5×10^{14}[a]	900–1200
1183.4	5×10^{14}[a]	1200
1186.5	5×10^{14}[a]	0 & 600

[a]Only studied at this fluence.

Some of the emission lines appear only in as-implanted samples and are located at 671.6, 822.2, 855.0, and 885.2 nm. Any heat treatment of the samples causes these defects to disappear, suggesting a very low thermal stability. Other emission lines, like those at 873.8–877.6 and 1186.5 nm, also exhibit relatively low thermal stabilities, disappearing at 300 and 600 °C, respectively. We speculate that candidates for these thermally unstable emission lines are less energetically favorable configurations of some of the primary intrinsic defects or small complexes thereof.

The group of emission lines between 873.8 and 877.6 nm, as shown in Fig. 5, is likely related as they have correlated temperature dependencies—enhanced brightness after the 300 °C anneal and disappearing at 600 °C and above. Furthermore, the lines are close-lying and have equidistant spacings around ~1.3 meV energy. As such, there is a similarity between these lines and the so-called L-lines (L1-L7) in 4H-SiC that were reported in Ref. 35, as they are spectrally close to the V1/V1' and have similar energetic spacing (1.4–1.5 meV). In the case of 4H-SiC, there is an assumption in the literature that the L-lines may be attributed to vibronic fine-structure of the $V_{Si}^{-}(h)$,[35] while another paper suggests that their origin comes from the perturbation of silicon vacancies caused by nearby carbon antisites (C_{Si}).[36] Thus, further studies of the L-lines in 6H-SiC might help shed more light on the origin of these defects.

A large fraction of the remaining unknown emission lines appear after annealing at 900–1200 °C. Interestingly, these lines appear in a temperature range where the $V_{Si}^{-}(h)$, CAV- and divacancy-complexes have started to disappear (see Fig. 1). This also coincides with the start of the mobility range of the carbon vacancy in 4H-SiC at 1100 °C.[37,38] Thus, the new emission lines may be complexes of the above-mentioned intrinsic defects that

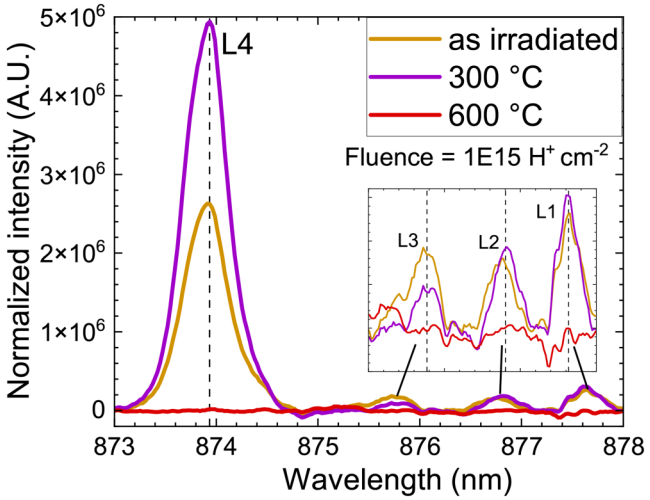

FIG. 5. PI emission at 10 K for the so-called L-lines in 6H-SiC from samples irradiated with 1×10^{15} H^{+} cm^{-2}, and annealed at 300 and 600 °C in Ar-flow for 30 min.

emit at different wavelengths than their previous states. It is also interesting to note that most of the defects that show up after the 1200 °C annealing step also disappear after annealing at even higher temperatures, suggesting that the defects are only stable for annealing around 1200 °C.

Lastly, we observe that there is a higher occurrence of defects that emit in certain regions of energy, such as 571–671, 746–885, and 1095–1186 nm, while other regions are completely free of color centers. Interestingly, the later two regions are close to where we find the three point defects that we have been studying previously, suggesting that they might be related. In particular, in the case of the last region (1095–1186 nm), most defects appear after an annealing at 1200 °C, suggesting that they might be involved in the disappearance of the divacancy complex at temperatures above 900 °C.

Interestingly, a similar phenomenon was observed in 4H-SiC, where the TS-lines were observed upon the disappearance of the divacancy and CAV pair.[39] The TS-defect has been tentatively assigned to a carbon di-vacancy-antisite complex that appears upon the out-annealing of the VV and CAV,[40] but further studies are needed to identify the origin of novel emission lines in 6H-SiC.

IV. CONCLUDING REMARKS

In this work, optical defect signatures in proton irradiated and annealed 4H- and 6H-SiC samples are investigated. In addition to the well known signatures of the V_{Si}, VV, and CAV defects, multiple sharp PL lines of unknown origin are observed both immediately after proton irradiation and following thermal treatments. We have studied the formation and annealing behavior of the VV, V_{Si}, and CAV defects in 6H-SiC and compared them to that of their 4H-SiC counterparts. It was found that there are many similarities for these defects in the two polytypes, including the proton fluence dependence of the CAV pair and the VV annealing dependence. There are, however, prominent differences, leading us to believe that the extra layer per stacking sequence in 6H-SiC affects the formation and stability of these point defects. As such, discrepancies in the behavior of these defects in the two polytypes emphasize the importance of looking into 6H-SiC as a potential QT-platform material. Specifically, the proton fluence dependencies for emission from the V_{Si} and VV defects differ between the polytypes, and it is unclear whether this should be attributed to the variations in the emission process, e.g., due to non-radiative channels, or to the differences in the defect formation probabilities in 4H- and 6H-SiC. Furthermore, the V_{Si} exhibits a scattered dependence on annealing temperature across configurations and polytypes, which requires further study to identify its optimal formation conditions for QT applications. Finally, the CAV pair shows the most distinct difference between the 4H and 6H cases, as it exhibits a clear maximum intensity after a 300 or 900 °C anneal in the 4H- and 6H-SiC samples, respectively, and disappears below the PL detection limit of our setup thereafter.

Overall CAV, V_{Si}, and VV mostly disappeared after annealing above 900 °C. This is accompanied by the appearance of multiple new and unknown emission lines that may be correlated with the disappearance of the known intrinsic defects. Further, not only are defect-related signals appearing after annealing above 900 °C, but we find a plethora of emission lines in the whole spectrum of fluences and temperatures that are likely intrinsic in origin. Further work is needed to determine their microscopic nature and possible viability for quantum technology applications.

ACKNOWLEDGMENTS

Financial support was kindly provided by the Research Council of Norway and the University of Oslo through the research project QuTe (No. 325573) and the Norwegian Micro- and Nano-Fabrication Facility, NorFab, Project No. 295864.

AUTHOR DECLARATIONS

Conflict of Interest

The authors have no conflicts to disclose.

Author Contributions

Erlend Lemva Ousdal: Conceptualization (equal); Data curation (lead); Formal analysis (lead); Investigation (lead); Methodology (equal); Validation (equal); Visualization (equal); Writing – original draft (lead). **Marianne Etzelmüller Bathen:** Conceptualization (equal); Funding acquisition (equal); Methodology (equal); Project administration (equal); Resources (equal); Supervision (equal); Validation (equal); Visualization (supporting); Writing – review & editing (lead). **Augustinas Galeckas:** Data curation (supporting); Formal analysis (supporting); Methodology (lead); Resources (equal); Writing – review & editing (supporting). **Andrej Kuznetsov:** Funding acquisition (equal); Methodology (equal); Resources (equal); Writing – review & editing (equal). **Lasse Vines:** Conceptualization (lead); Funding acquisition (equal); Methodology (equal); Project administration (lead); Resources (equal); Supervision (equal); Validation (equal); Writing – review & editing (equal).

DATA AVAILABILITY

The data that support the findings of this study are available from the corresponding author upon reasonable request.

REFERENCES

[1]T. Kimoto and J. A. Cooper, *Fundamentals of Silicon Carbide Technology: Growth, Characterization, Devices and Applications* (Wiley, 2014).
[2]P. B. Klein, B. V. Shanabrook, S. W. Huh, A. Y. Polyakov, M. Skowronski, J. J. Sumakeris, and M. J. O'Loughlin, "Lifetime-limiting defects in n-4H-SiC epilayers," Appl. Phys. Lett. **88**, 052110 (2006).
[3]K. Danno, D. Nakamura, and T. Kimoto, "Investigation of carrier lifetime in 4H-SiC epilayers and lifetime control by electron irradiation," Appl. Phys. Lett. **90**, 202109 (2007).
[4]M. Ghezellou, P. Kumar, M. E. Bathen, R. Karsthof, E. Ö. Sveinbjörnsson, U. Grossner, J. P. Bergman, L. Vines, and J. Ul-Hassan, "The role of boron related defects in limiting charge carrier lifetime in 4H-SiC epitaxial layers," APL Mater. **11**, 031107 (2023).
[5]C. Martinella, M. E. Bathen, A. Javanainen, and U. Grossner, "Heavy-ion-induced defects in degraded SiC power MOSFETs," Mater. Sci. Forum **1090**, 179–184 (2023).
[6]J. Müting and U. Grossner, "Simulation-based sensitivity analysis of conduction and switching losses for silicon carbide power MOSFETs," in *Silicon Carbide*

and Related Materials 2017, Materials Science Forum Vol. 924 (Trans Tech Publications Ltd, 2018), pp. 693–696.
[7]S. Castelletto, L. Rosa, and B. C. Johnson, "Silicon carbide for novel quantum technology devices," in *Advanced Silicon Carbide Devices and Processing* (InTech, 2015).
[8]S. Castelletto, B. C. Johnson, V. Ivády, N. Stavrias, T. Umeda, A. Gali, and T. Oshima, "A silicon carbide room-temperature single-photon source," Nat. Mater. **13**, 151–156 (2014).
[9]M. Widmann, S.-Y. Lee, T. Rendler, N. T. Son, H. Fedder, S. Paik, L.-P. Yang, N. Zhao, S. Yang, I. Booker, A. Denisenko, M. Jamali, S. A. Momenzadeh, I. Gerhardt, T. Ohshima, A. Gali, E. Janzén, and J. Wrachtrup, "Coherent control of single spins in silicon carbide at room temperature," Nat. Mater. **14**, 164–168 (2015).
[10]D. J. Christle, A. L. Falk, P. Andrich, P. V. Klimov, J. Ul Hassan, N. T. Son, E. Janzén, T. Oshima, and D. D. Awschalom, "Isolated electron spins in silicon carbide with millisecond coherence times," Nat. Mater. **14**, 160–163 (2015).
[11]Z. Mu, S. A. Zargaleh, H. J. von Bardeleben, J. E. Fröch, M. Nonahal, H. Cai, X. Yang, J. Yang, X. Li, I. Aharonovich, and W. Gao, "Coherent manipulation with resonant excitation and single emitter creation of nitrogen vacancy centers in 4H silicon carbide," Nano Lett. **20**, 6142–6147 (2020).
[12]N. Iwamoto and B. G. Svensson, "Chapter ten - Point defects in silicon carbide," in *Defects in Semiconductors*, Semiconductors and Semimetals Vol. 91, edited by L. Romano, V. Privitera, and C. Jagadish (Elsevier, 2015), pp. 369–407.
[13]J. Coutinho, "Theory of the thermal stability of silicon vacancies and interstitials in 4H-SiC," Crystals **11**, 167 (2021).
[14]M. E. Bathen, A. Galeckas, J. Müting, H. M. Ayedh, U. Grossner, J. Coutinho, Y. K. Frodason, and L. Vines, "Electrical charge state identification and control for the silicon vacancy in 4H-SiC," npj Quantum Inf. **5**, 111 (2019).
[15]S. G. Sundaresan, N. A. Mahadik, S. B. Qadri, J. A. Schreifels, Y.-L. Tian, Q. Zhang, E. Gomar-Nadal, and M. V. Rao, "Ultra-low resistivity Al^+ implanted 4H-SiC obtained by microwave annealing and a protective graphite cap," Solid-State Electron. **52**, 140–145 (2008).
[16]Y. Negoro, K. Katsumoto, T. Kimoto, and H. Matsunami, "Electronic behaviors of high-dose phosphorus-ion implanted 4H-SiC (0001)," J. Appl. Phys. **96**, 224–228 (2004).
[17]R. Karsthof, M. Etzelmüller Bathen, A. Kuznetsov, and L. Vines, "Formation of carbon interstitial-related defect levels by thermal injection of carbon into n-type 4H-SiC," J. Appl. Phys. **131**, 035702 (2022).
[18]M. E. Bathen, R. Karsthof, A. Galeckas, P. Kumar, A. Y. Kuznetsov, U. Grossner, and L. Vines, "Impact of carbon injection in 4H-SiC on defect formation and minority carrier lifetime," Mater. Sci. Semicond. Process. **176**, 108316 (2024).
[19]J. W. Steeds, "Photoluminescence study of the carbon antisite-vacancy pair in 4H- and 6H-SiC," Phys. Rev. B **80**, 245202 (2009).
[20]S. Castelletto and A. Boretti, "Silicon carbide color centers for quantum applications," J. Phys.: Photonics **2**, 022001 (2020).
[21]E. Sörman, N. T. Son, W. M. Chen, O. Kordina, C. Hallin, and E. Janzén, "Silicon vacancy related defect in 4H and 6H SiC," Phys. Rev. B **61**, 2613–2620 (2000).
[22]M. Wagner, B. Magnusson, W. M. Chen, E. Janzén, E. Sörman, C. Hallin, and J. L. Lindström, "Electronic structure of the neutral silicon vacancy in 4H and 6H SiC," Phys. Rev. B **62**, 16555–16560 (2000).
[23]E. Janzén, A. Gali, P. Carlsson, A. Gällström, B. Magnusson, and N. Son, "The silicon vacancy in SiC," Physica B **404**, 4354–4358 (2009).
[24]N. T. Son *et al.*, "Developing silicon carbide for quantum spintronics," Appl. Phys. Lett. **116**, 190501 (2020).
[25]A. L. Falk, B. B. Buckley, G. Calusine, W. F. Koehl, V. V. Dobrovitski, A. Politi, C. A. Zorman, P. X.-L. Feng, and D. D. Awschalom, "Polytype control of spin qubits in silicon carbide," Nat. Commun. **4**, 1819 (2013).
[26]J. Davidsson, V. Ivády, R. Armiento, T. Ohshima, N. T. Son, A. Gali, and I. A. Abrikosov, "Identification of divacancy and silicon vacancy qubits in 6H-SiC," Appl. Phys. Lett. **114**, 112107 (2019).
[27]V. Ivády, J. Davidsson, N. T. Son, T. Ohshima, I. A. Abrikosov, and A. Gali, "Identification of si-vacancy related room-temperature qubits in 4H silicon carbide," Phys. Rev. B **96**, 161114 (2017).
[28]J. Davidsson, V. Ivády, R. Armiento, N. T. Son, A. Gali, and I. A. Abrikosov, "First principles predictions of magneto-optical data for semiconductor point defect identification: The case of divacancy defects in 4H-SiC," New J. Phys. **20**, 023035 (2018).
[29]J. W. Steeds, "Photoluminescence study of the carbon antisite-vacancy pair in 4H- and 6H-SiC," Phys. Rev. B **80**, 245202 (2009).
[30]C. Haberstroh, R. Helbig, and R. A. Stein, "Some new features of the photoluminescence of SiC(6H), SiC(4H), and SiC(15R)," J. Appl. Phys. **76**, 509–513 (1994).
[31]E. M. Y. Lee, A. Yu, J. J. de Pablo, and G. Galli, "Stability and molecular pathways to the formation of spin defects in silicon carbide," Nat. Commun. **12**, 6325 (2021).
[32]M. E. Bathen, J. Coutinho, H. M. Ayedh, J. Ul Hassan, I. Farkas, S. Öberg, Y. K. Frodason, B. G. Svensson, and L. Vines, "Anisotropic and plane-selective migration of the carbon vacancy in SiC: Theory and experiment," Phys. Rev. B **100**, 014103 (2019).
[33]A. F. M. Almutairi, J. G. Partridge, C. Xu, I. S. Cole, and A. S. Holland, "Direct writing of divacancy centers in silicon carbide by femtosecond laser irradiation and subsequent thermal annealing," Appl. Phys. Lett. **120**, 014003 (2022).
[34]I. D. Breev, Z. Shang, A. V. Poshakinskiy, H. Singh, Y. Berencén, M. Hollenbach, S. S. Nagalyuk, E. N. Mokhov, R. A. Babunts, P. G. Baranov, D. Suter, S. A. Tarasenko, G. V. Astakhov, and A. N. Anisimov, "Inverted fine structure of a 6H-SiC qubit enabling robust spin-photon interface," npj Quantum Inf. **8**, 23 (2022).
[35]M. E. Bathen, A. Galeckas, R. Karsthof, A. Delteil, V. Sallet, A. Y. Kuznetsov, and L. Vines, "Resolving jahn-teller induced vibronic fine structure of silicon vacancy quantum emission in silicon carbide," Phys. Rev. B **104**, 045120 (2021).
[36]J. Davidsson, R. Babar, D. Shafizadeh, V. I. I. Ivanov, R. Armiento, and I. Abrikosov, "Exhaustive characterization of modified si vacancies in 4H-SiC," Nanophotonics **11**, 4565 (2022).
[37]T. Umeda, J. Isoya, N. Morishita, T. Ohshima, T. Kamiya, A. Gali, P. Deák, N. T. Son, and E. Janzén, "EPR and theoretical studies of positively charged carbon vacancy in 4H-SiC," Phys. Rev. B **70**, 235212 (2004).
[38]M. E. Bathen, J. Coutinho, H. M. Ayedh, J. Ul Hassan, I. Farkas, S. Öberg, Y. K. Frodason, B. G. Svensson, and L. Vines, "Anisotropic and plane-selective migration of the carbon vacancy in SiC: Theory and experiment," Phys. Rev. B **100**, 014103 (2019).
[39]M. Rühl, C. Ott, S. Götzinger, M. Krieger, and H. B. Weber, "Controlled generation of intrinsic near-infrared color centers in 4H-SiC via proton irradiation and annealing," Appl. Phys. Lett. **113**, 122102 (2018).
[40]M. Schober, N. Jungwirth, T. Kobayashi, J. A. Lehmeyer, M. Krieger, H. B. Weber, and M. Bockstedte, "The optical properties of the carbon di-vacancy-antisite complex in the light of the ts photoluminescence center," Defect Diffus. Forum **426**, 43–48 (2023).